

Supporting Information

Photocatalytic co-production of hydrogen gas and N-benzylidenebenzylamine over high-quality 2D layered $\text{In}_{4/3}\text{P}_2\text{Se}_6$ nanosheet

Binglan Wu^{1,2†}, Xueying Zhan^{2†}, Peng Yu^{2†}, Jun Meng³, Marshet Getaye Sendeku², Fekadu Tsegaye Dajan², Ning Gao², Wenjia Lai², Ying Yang^{1,*}, Zhenxing Wang² and Fengmei Wang^{2,*}

¹Shaanxi Provincial Key Laboratory of Electroanalytical Chemistry, Key Laboratory of Synthetic and Natural Functional Molecule Chemistry of the Ministry of Education, College of Chemistry & Materials Science, Northwest University, Xi'an, 710127, China

²CAS Center for Excellence in Nanoscience, CAS Key Laboratory of Nanosystem and Hierarchical Fabrication, National Center for Nanoscience and Technology, Beijing 100190, China

³Division of Interfacial Water and Key Laboratory of Interfacial Physics and Technology, Shanghai Institute of Applied Physics, Chinese Academy of Sciences, Shanghai 201800, P. R. China

[†]These authors contributed equally.

E-mail: yingyang@nwu.edu.cn, wangfm@nanoctr.cn

Note S1

Synthesis of In_2S_3 precursor. The In_2S_3 precursor on carbon cloth was synthesized by a facile solvothermal method. Firstly, a stoichiometric mixture of 2.0 mmol InCl_3 and 8.0 mmol thioacetamide was dispersed in 40 mL absolute ethanol and then transferred to a Teflon-lined stainless-steel autoclave. Then, a piece of carbon cloth with the size of 4 cm \times 2 cm was immersed into the solution and heated at 70 °C for 18 h to synthesize In_2S_3 nanosheets on the surface of carbon cloth. After naturally cooling to room temperature, the carbon cloth loaded with the In_2S_3 precursor was taken out and rinsed using deionized water and ethanol several times, and finally dried at 65 °C for further experiments.

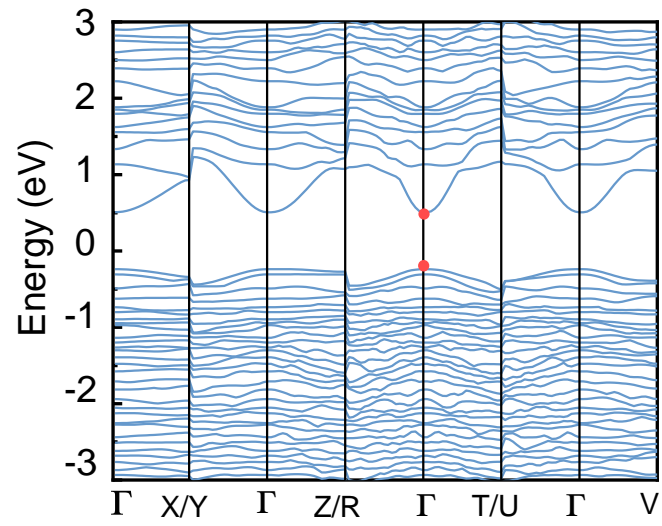


Fig. S1. The calculated band structure of $\text{In}_{4/3}\text{P}_2\text{Se}_6$ using Perdew-Burke-Ernzerhof (PBE) functional.

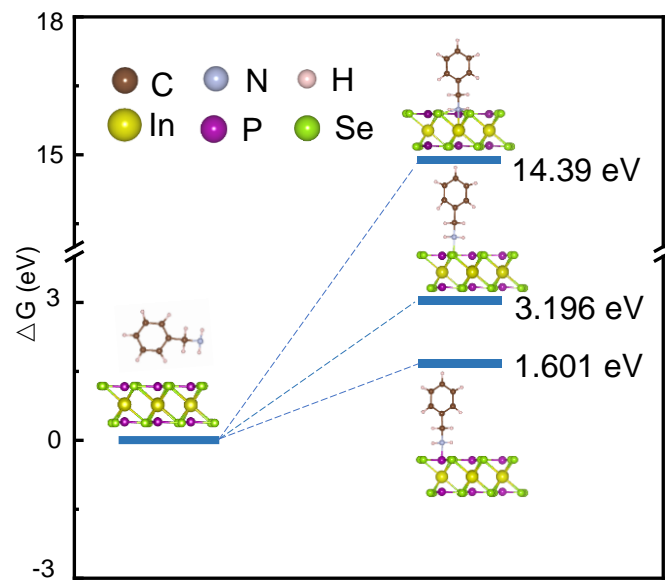


Fig. S2 Adsorption energies of benzylamine molecular on In, P and Se sites of $\text{In}_{4/3}\text{P}_2\text{Se}_6$ monolayer.

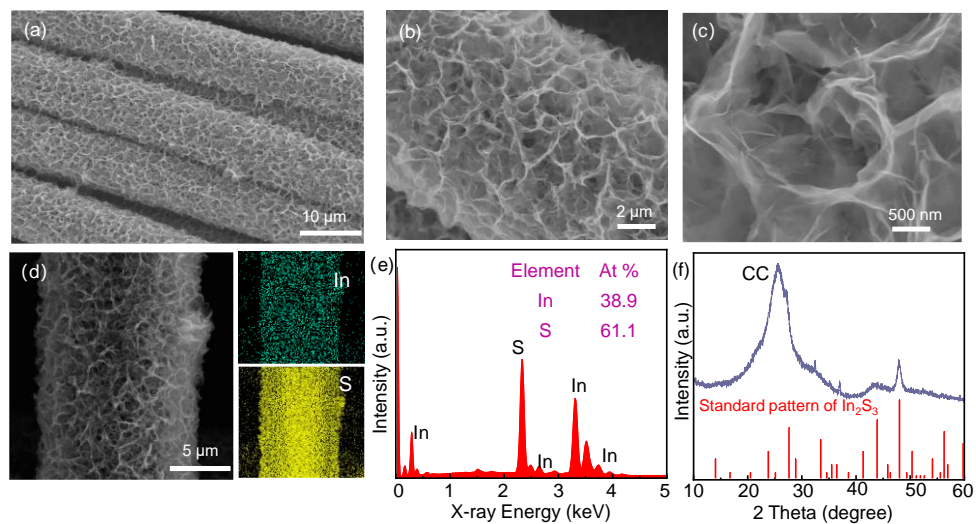


Fig. S3 (a-c) Low- and high-magnification SEM images of In_2S_3 nanosheets grown on carbon cloth. (d-e) EDX elemental mappings (d) and spectrum (e) of In and S in the In_2S_3 nanosheets on carbon cloth. (f) XRD pattern of In_2S_3 nanosheets grown on carbon cloth.

From the SEM images in Fig. S3, the In_2S_3 nanosheets were evenly distributed on the surface of carbon cloth, showing a honeycomb-like nanosheet structure. The energy dispersive X-ray spectrum (EDX) mapping also showed that the whole surface of carbon cloth was uniformly covered by In_2S_3 nanosheets with the In: S element ratio of 2:3 (Fig. S3d-e). X-ray diffraction (XRD) pattern (Fig. S3f) shows an obvious diffraction peak at 47.9° , assigned to the (440) crystal plane of cubic In_2S_3 (PDF#32-0456) crystal.

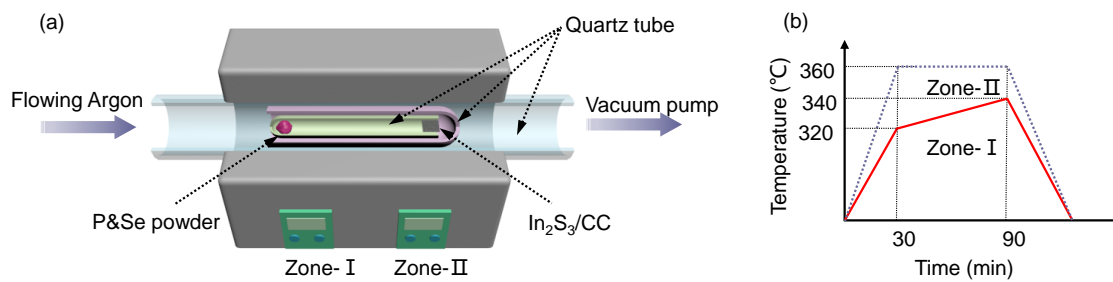


Fig. S4 Schematic of space confined chemical vapor conversion method with tube furnace for $\text{In}_{4/3}\text{P}_2\text{Se}_6$ nanosheet synthesis ("CC" in (a) denotes as carbon cloth).

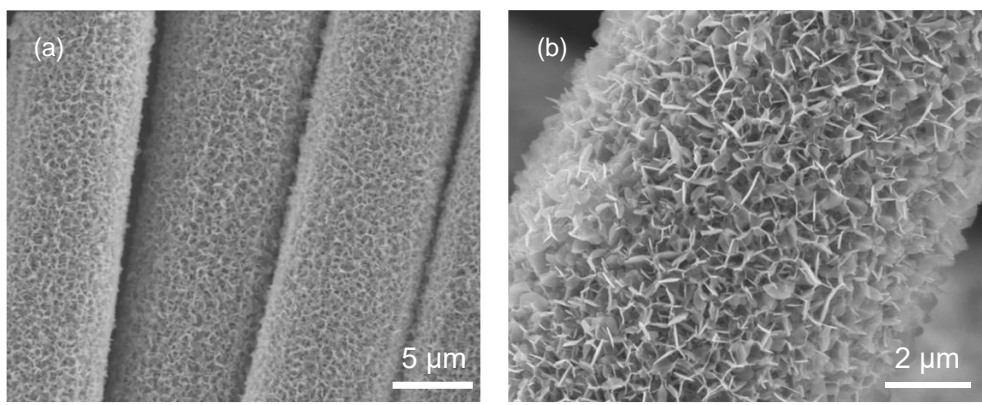


Fig. S5 Low-magnification SEM images of $\text{In}_{4/3}\text{P}_2\text{Se}_6$ nanosheets grown on carbon cloth.

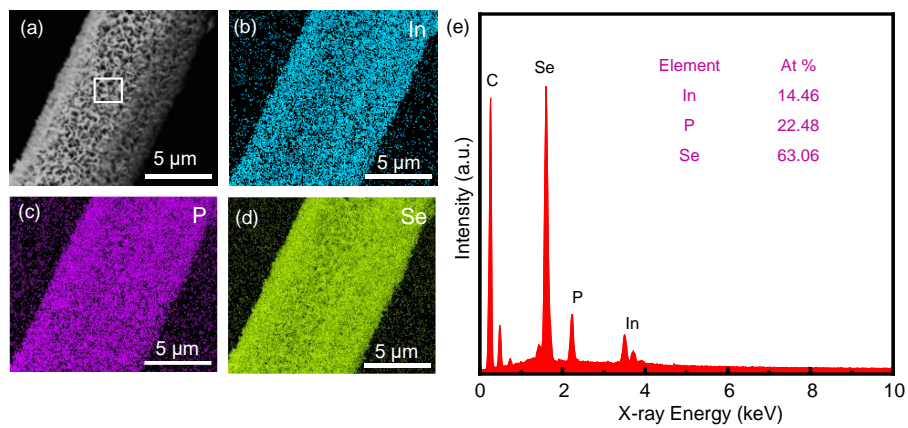


Fig. S6 (a) SEM image of $\text{In}_{4/3}\text{P}_2\text{Se}_6$ nanosheets grown on one carbon fiber of the carbon cloth. (b-d) EDX elemental mappings of In, P and Se of the $\text{In}_{4/3}\text{P}_2\text{Se}_6$ nanosheets grown on one carbon fiber of the carbon cloth. (e) EDX spectrum collected from marked region in a, showing the atomic ratio of In: P: Se as 1: 1.5: 4.4.

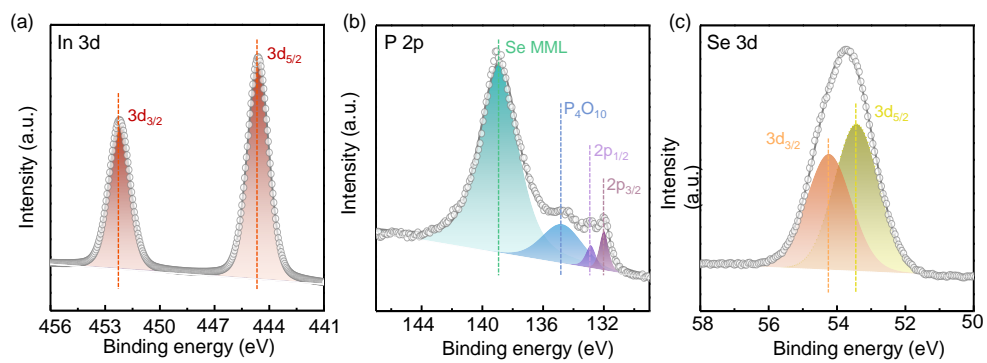


Fig. S7 XPS high-resolution scans of In 3d, P 2p and Se 3d regions in the $In_{4/3}P_2Se_6$ nanosheet sample.

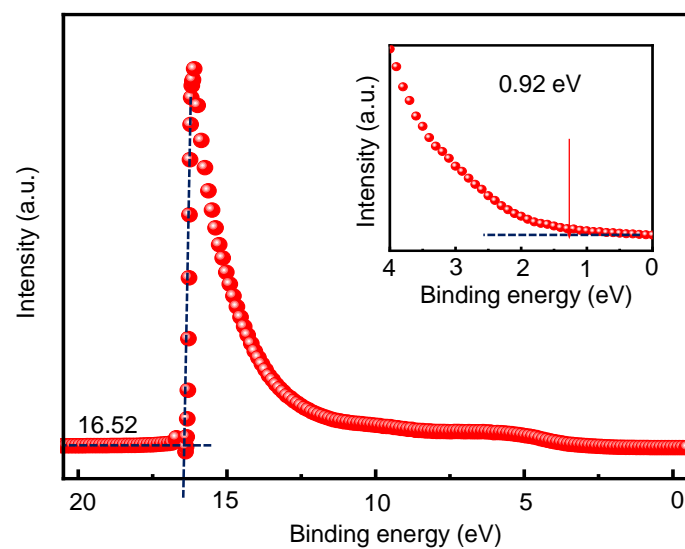


Fig. S8 UPS spectrum of the $\text{In}_{4/3}\text{P}_2\text{Se}_6$ nanosheet film on indium tin oxide (ITO) glass. From this UPS spectrum, the VBM level of $\text{In}_{4/3}\text{P}_2\text{Se}_6$ is estimated to be at 1.18 V versus NHE (-5.62 eV vs Vacuum level, which is calculated by subtracting the He I photon energy (21.22 eV); the CBM can be then calculated by using $E_{\text{CB}} = E_{\text{VB}} - E_{\text{g}}$, which is estimated to be at -0.76 V versus NHE (-3.68 eV vs Vacuum level).^{1,2}

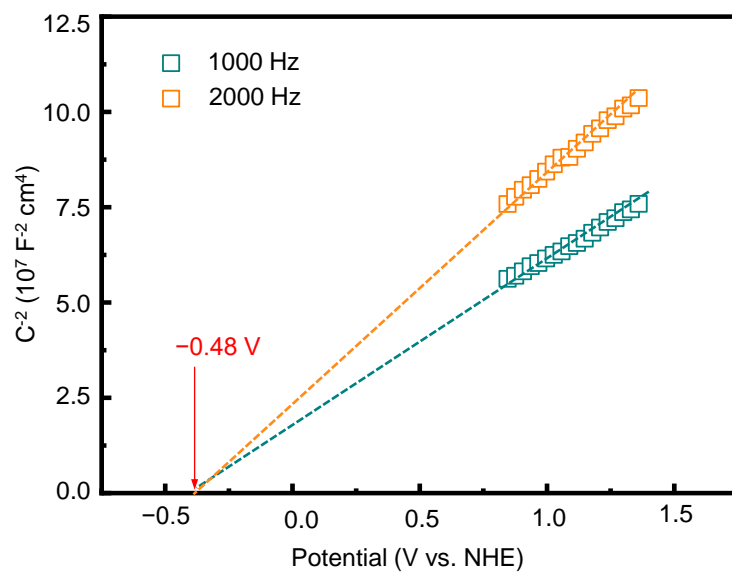


Fig. S9 Mott-Schottky plots for the $\text{In}_{4/3}\text{P}_2\text{Se}_6$ electrode at 1000 and 2000 Hz frequencies.

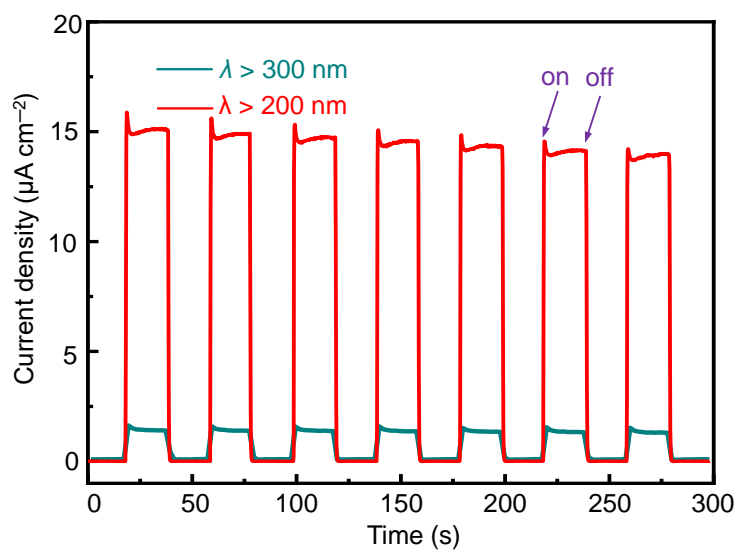


Fig. S10 Transient photocurrent responses of $\text{In}_{4/3}\text{P}_2\text{Se}_6$ nanosheet photoelectrode measured in 0.5 M Na_2SO_4 aqueous solution under different Xenon light illumination with the same power density of 200 mW cm^{-2} .

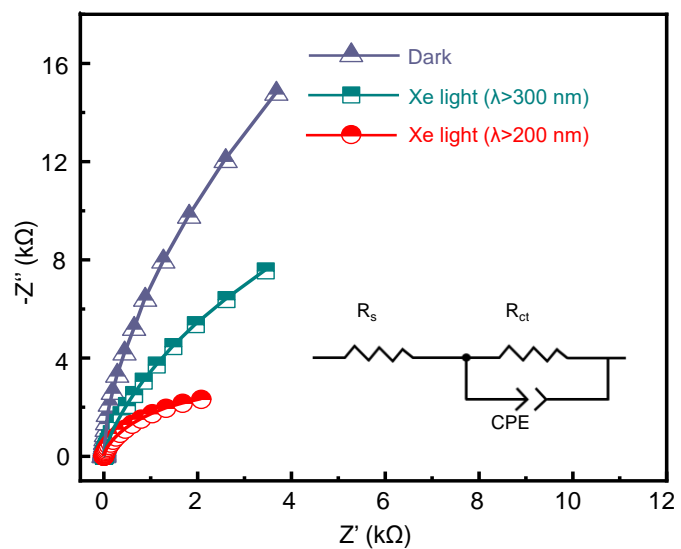


Fig. S11 EIS Nyquist plots of $\text{In}_{4/3}\text{P}_2\text{Se}_6$ nanosheet photoelectrode measured in $0.5 \text{ M Na}_2\text{SO}_4$ electrolyte under different Xenon light illumination with the same power density of 200 mW cm^{-2} .

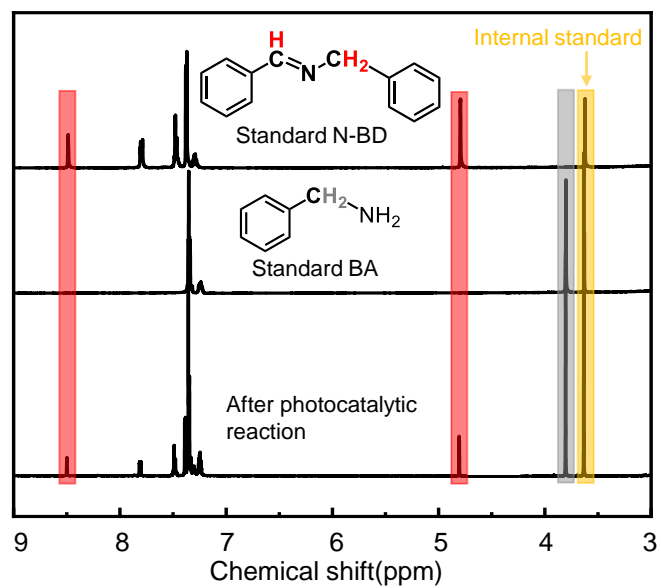


Fig. S12 ^1H NMR spectra of the standard N-BD, standard BA, combined with the ^1H NMR collected from the reaction solution after the photo-oxidation coupling reaction using $\text{In}_{4/3}\text{P}_2\text{Se}_6$ nanosheet photocatalyst.

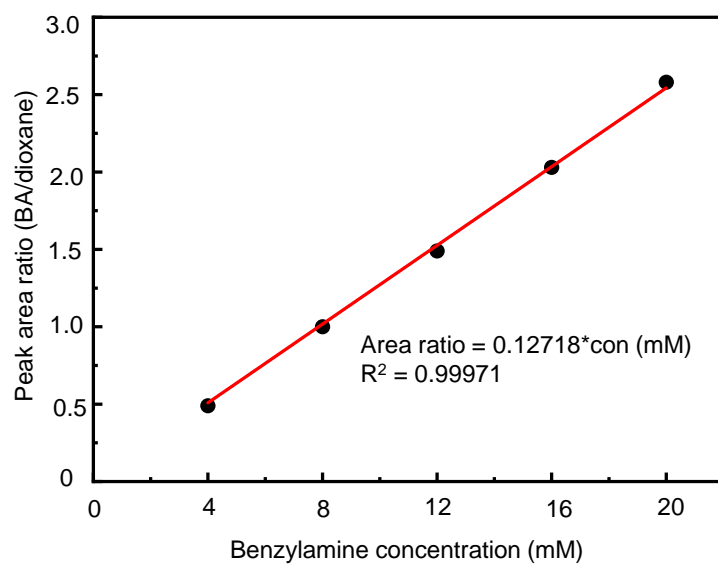


Fig. S13 Calibration curve obtained based on the various concentrated benzylamine analyzed by ¹H NMR.

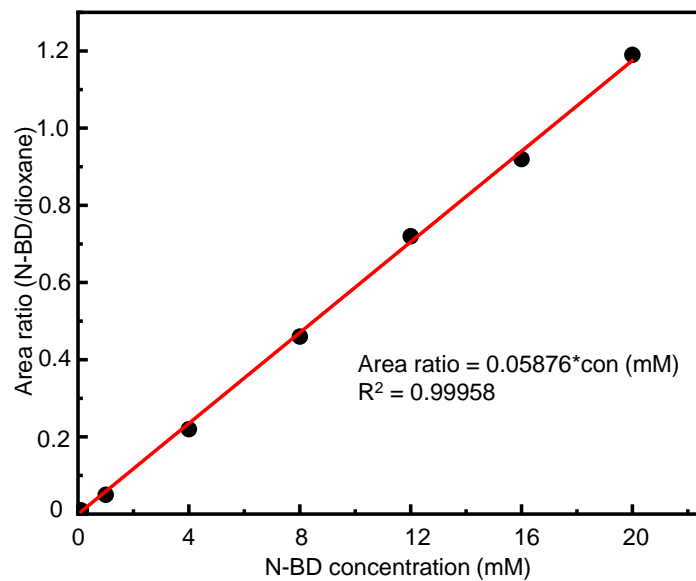


Fig. S14 Calibration curve obtained based on the various concentrated N-BD analyzed by ^1H NMR spectrum.

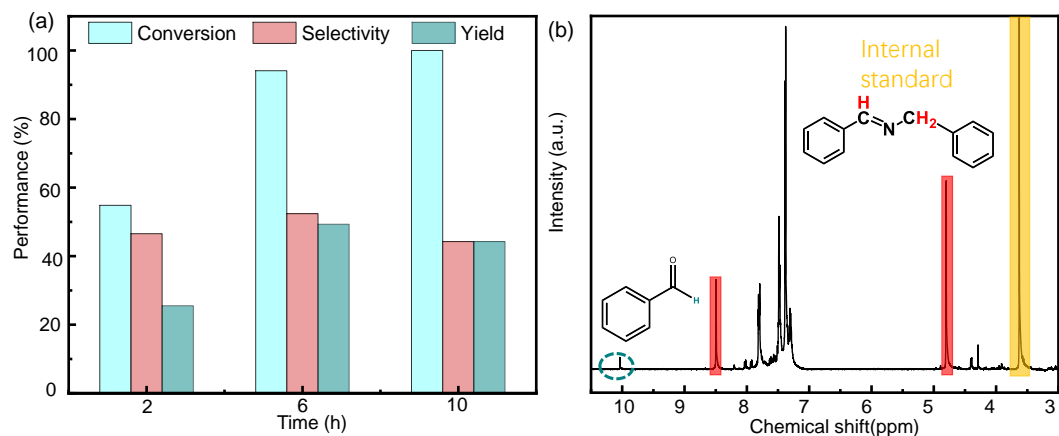


Fig. S15 Photocatalytic oxidative transformation of BA to N-BD by using xenon light source ($\lambda > 200$ nm, 200 mW cm^{-2}) in 10 mL acetonitrile, using 20 mg catalyst with 0.2 mmol BA substrate under ambient condition at room temperature. (a) Time-dependent BA conversion, N-BD selectivity and corresponding yield over $\text{In}_{4/3}\text{P}_2\text{Se}_6$ under Xenon light illumination. (b) ^1H NMR spectra collected from the solution after 10 h photo-oxidation coupling reaction over $\text{In}_{4/3}\text{P}_2\text{Se}_6$ nanosheet photocatalyst.

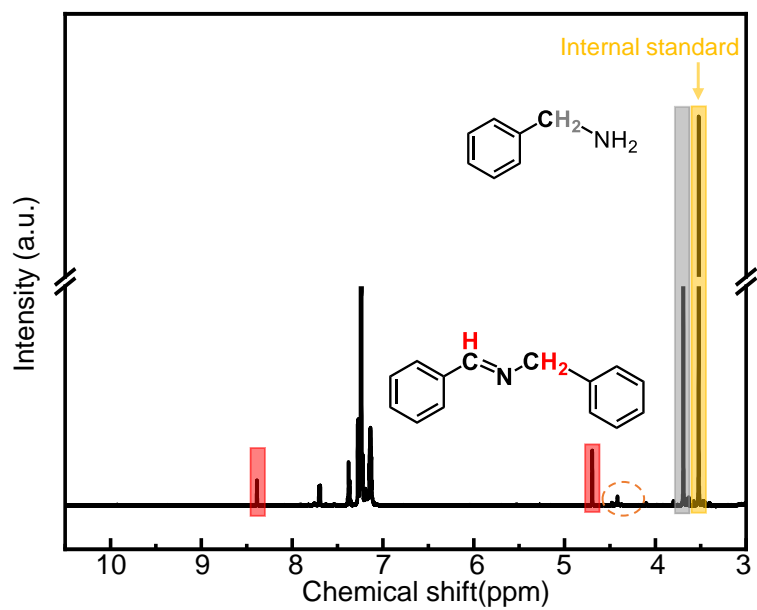


Fig. S16 Corresponding ^1H NMR spectra collected from the anaerobic oxidative coupling of BA in the condition of 20 mL acetonitrile, 100 μL H_2O , 20 mg catalyst and 0.2 mmol BA substrate under anaerobic condition at room temperature, illuminated by a 300 W xenon lamp ($\lambda > 300 \text{ nm}$, 200 mW cm^{-2}) for 16 h, with dioxane as internal standard.

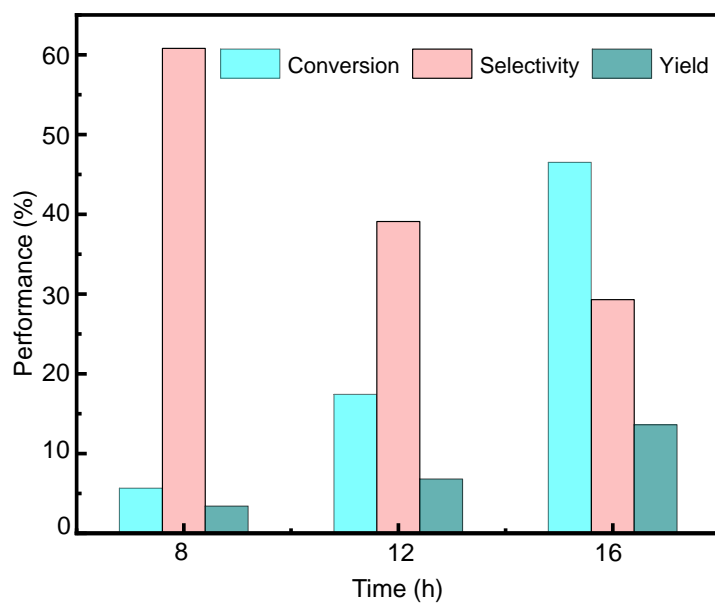


Fig. S17 Time-dependent photocatalytic oxidative transformation of BA to N-BD in 20 mL acetonitrile and 100 μL H_2O , using 20 mg catalyst with 0.2 mmol BA substrate under anaerobic condition at room temperature. N-BD yield, selectivity and corresponding conversion of BA over $\text{In}_{4/3}\text{P}_2\text{Se}_6$ under Xenon light illumination ($\lambda > 300 \text{ nm}$, 200 mW cm^{-2}) were collected.

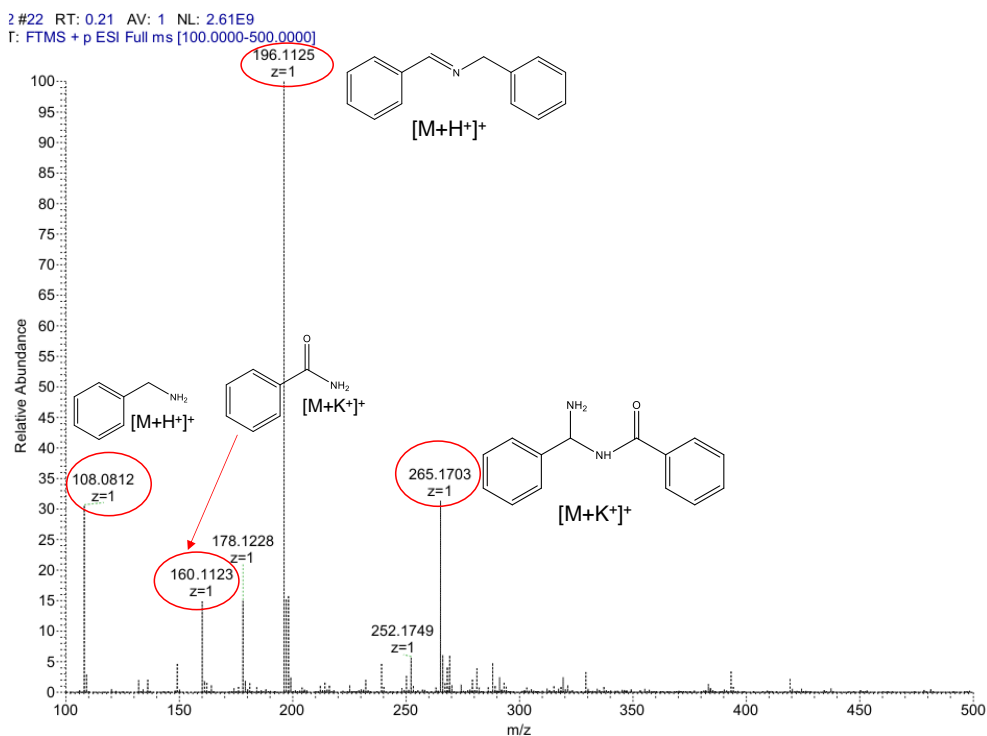


Fig. S18 Mass spectrogram analysis of the reaction solution collected after the 16 h continuous reaction under anaerobic condition. Reaction condition: 20 mg catalyst and 0.2 mmol BA substrate in 20 mL acetonitrile and 100 μ L H₂O, illuminated by a 300 W Xenon lamp ($\lambda > 300$ nm, 200 mW cm⁻²).

Prior to the high-resolution mass spectrogram analysis, the reaction solution was qualitatively analyzed based on the characteristic fragment ion peaks (FIPs) after separating the catalyst through centrifugal process. The peaks at 108.0812, 196.1125, 160.1123 and 265.1703 shown in Fig. S12 reveal the existence of BA, N-BD and the byproduct of benzamide ([M + K]⁺) and N-(amino(phenyl)methyl)benzamide ([M + K]⁺) in the final reaction solution, respectively. It is worth noting that the byproduct benzamide can be attributed to the dehydrogenation of the imine intermediate generated in the reaction step (III) (Figure 4b) to benzonitrile, which further reacts with water to form benzamide³.

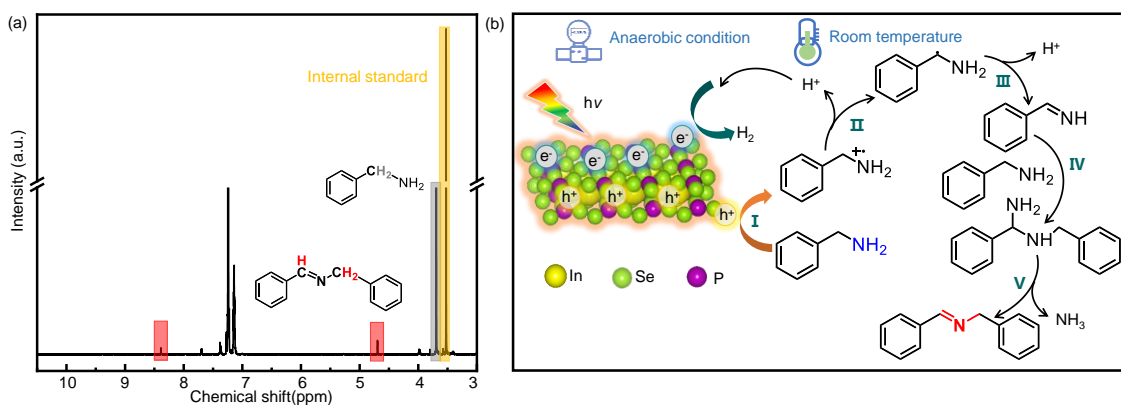


Fig. S19 Control photocatalytic test over $\text{In}_{4/3}\text{P}_2\text{Se}_6$ nanosheet catalyst only in acetonitrile solvent under anaerobic condition. Reaction conditions: acetonitrile (20 mL), catalyst (20 mg), with BA substrate (0.2 mmol) at room temperature, the reactor was firstly evacuated and no detectable dissolved oxygen gas in the reactor. (a) Corresponding ^1H NMR spectra collected from the reaction solution after 10 h continuous reaction, with dioxane as internal standard. (b) Proposed reaction mechanism for the photocatalytic oxidative transformation of BA to N-BD catalyzed by $\text{In}_{4/3}\text{P}_2\text{Se}_6$ nanosheet without air or O_2 involvement in pure acetonitrile solvent.

As a comparison, we also studied the photocatalytic BA oxidation only in acetonitrile under the same anaerobic condition. From the ^1H -NMR analysis in Fig. S19a, we can conclude that the N-BD chemical could be synthesized after 10 h continuous reaction based on the peaks at 4.7 ppm and 8.38 ppm. Meanwhile, some amount of hydrogen gas ($22 \mu\text{mol g}^{-1}$) was also detected through the on-line gas chromatography analysis. Thus, a different reaction mechanism^{4, 5} was proposed in Figure S19b. The released protons from the step II would further react with the photogenerated electrons to produce the hydrogen gas. Note that the benzylamine radical could be then deprotonated to form carbon radical and imine intermediate (step II and III), which is different with the reaction mechanisms under other two conditions.

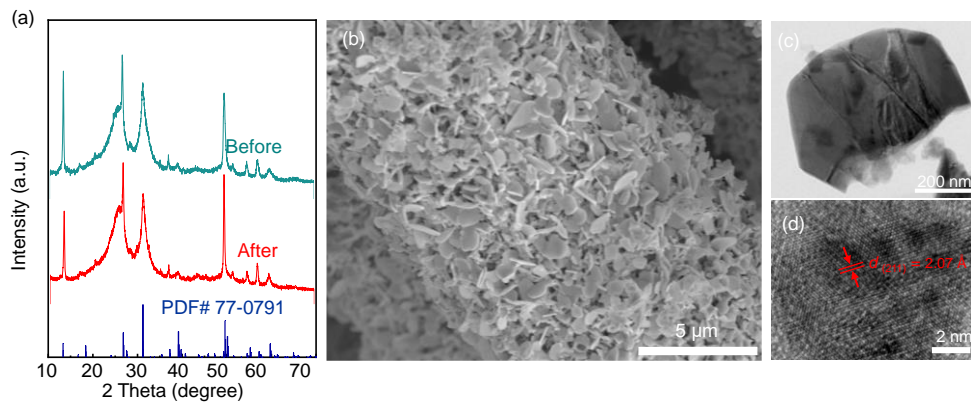


Fig. S20 Structural characterizations of $\text{In}_{4/3}\text{P}_2\text{Se}_6$ nanosheets after water photocatalysis for H_2 evolution under Xenon light ($\lambda > 200 \text{ nm}$, 200 mW cm^{-2}) illumination for 24-hour reaction. (a) Comparison of XRD patterns of $\text{In}_{4/3}\text{P}_2\text{Se}_6$ nanosheets before and after photocatalytic H_2 evolution measurement. (b-d) SEM, TEM and HRTEM images of $\text{In}_{4/3}\text{P}_2\text{Se}_6$ nanosheet after water photocatalysis.

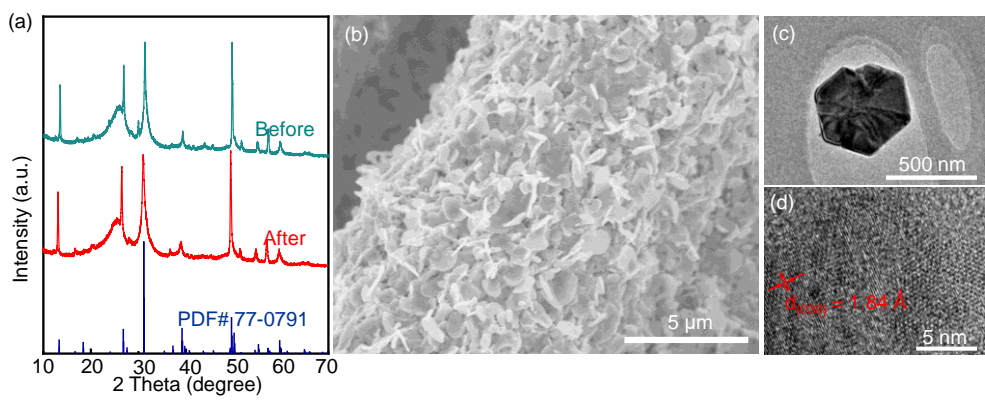


Fig. S21 Structural characterization of $\text{In}_{4/3}\text{P}_2\text{Se}_6$ nanosheets after photocatalytic oxidation of benzylamine under Xenon light illumination ($\lambda > 300 \text{ nm}$, 200 mW cm^{-2}) for 10 h continuous reaction. (a) Comparison of XRD patterns of $\text{In}_{4/3}\text{P}_2\text{Se}_6$ nanosheets before and after photocatalytic oxidation benzylamine. (b-d) SEM, TEM and HRTEM images of $\text{In}_{4/3}\text{P}_2\text{Se}_6$ nanosheet after photocatalytic oxidation of benzylamine.

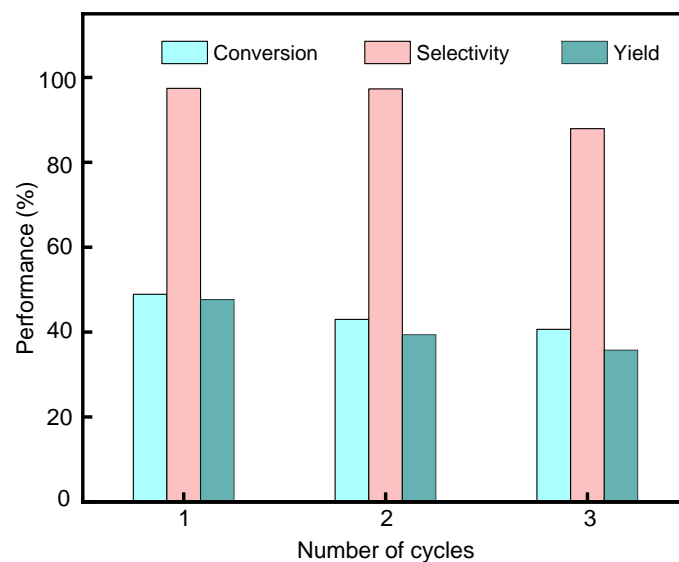


Fig. S22 Recycling performance of the $\text{In}_{4/3}\text{P}_2\text{Se}_6$ nanosheet catalyst for photocatalytic oxidation of BA. Reaction conditions: 20 mg catalyst, 10 mL CH_3CN , 0.2 mmol BA, illuminated under Xenon light ($\lambda > 300$ nm, 200 mW cm^{-2}) with continuous stirring at room temperature for 10 h in each cycle.

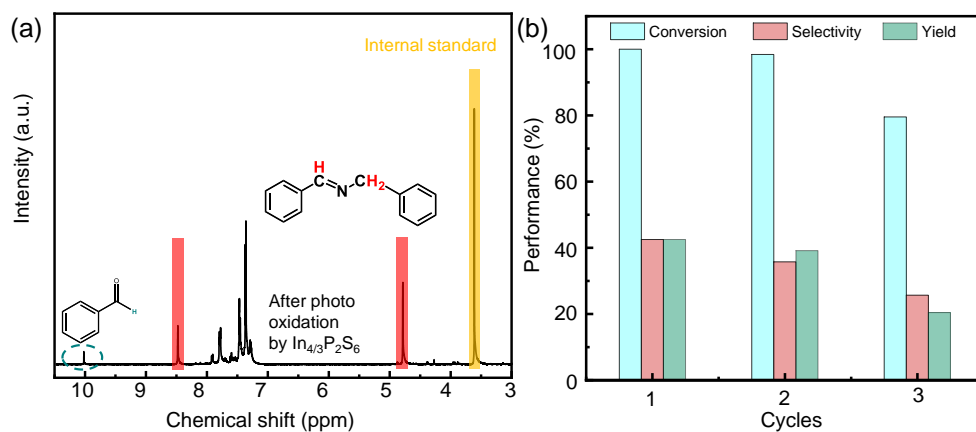


Fig. S23 Photocatalytic oxidative transformation of BA to N-BD over In_{4/3}P₂S₆ nanosheet in 10 mL acetonitrile, using 20 mg catalyst with 0.2 mmol BA substrate under ambient condition at room temperature by using Xenon light ($\lambda > 300$ nm, 200 mW cm⁻²). (a) ¹H NMR spectra collected from the solution after 10 h photo-oxidation coupling reaction. (b) Recycling performance of the In_{4/3}P₂S₆ nanosheet catalyst for photocatalytic oxidation of BA to N-BD with continuous stirring for 10 h in each cycle.

Table S1. Comparison of the experimental and calculated crystal parameters of $\text{In}_{4/3}\text{P}_2\text{Se}_6$.

| Crystal parameters | Refined results | Calculation results |
|--------------------|-----------------|---------------------|
| a | 6.292 Å | 6.362 Å |
| b | 6.292 Å | 6.362 Å |
| c | 20.163 Å | 19.929 Å |
| α | 90° | 90° |
| β | 90° | 90° |
| γ | 120° | 120° |

References

1. M. G. Sendeku, F. Wang, Z. Cheng, P. Yu, N. Gao, X. Zhan, Z. Wang and J. He, *ACS Appl. Mater. Interfaces*, 2021, **13**, 13392-13399.
2. R. Nechache, C. Harnagea, S. Li, L. Cardenas, W. Huang, J. Chakrabartty and F. Rosei, *Nat. Photonics*, 2015, **9**, 61-67.
3. C. Wu, J. Bu, W. Wang, H. Shen, Y. Cao and H. Zhang, *Ind. Eng. Chem. Res.*, 2022, **61**, 5442-5452.
4. Y. Huang, C. Liu, M. Li, H. Li, Y. Li, R. Su and B. Zhang, *ACS Catal*, 2020, **10**, 3904-3910.
5. H. Wang, P. Hu, J. Zhou, M. B. Roeffaers, B. Weng, Y. Wang and H. Ji, *J. Mater. Chem. A*, 2021, **9**, 19984-19993.